

ELAA Near-Field Localization and Sensing with Partial Blockage Detection

Hui Chen*, Pinjun Zheng[†], Yu Ge*, Ahmed Elzanaty[‡], Jiguang He[§], Tareq Y. Al-Naffouri[†], Henk Wymeersch*

*Chalmers University of Technology, Sweden [†]King Abdullah University of Science and Technology, KSA

[‡]University of Surrey, UK [§]Technology Innovation Institute, UAE

Abstract—High-frequency communication systems bring extremely large aperture arrays (ELAA) and large bandwidths, integrating localization and (bi-static) sensing functions without extra infrastructure. Such systems are likely to operate in the near-field (NF), where the performance of localization and sensing is degraded if a simplified far-field channel model is considered. However, when taking advantage of the additional geometry information in the NF, e.g., the encapsulated information in the wavefront, localization and sensing performance can be improved. In this work, we formulate a joint synchronization, localization, and sensing problem in the NF. Considering the array size could be much larger than an obstacle, the effect of partial blockage (i.e., a portion of antennas are blocked) is investigated, and a blockage detection algorithm is proposed. The simulation results show that blockage greatly impacts performance for certain positions, and the proposed blockage detection algorithm can mitigate this impact by identifying the blocked antennas.

Index Terms—Near field, localization, sensing, partial blockage, extremely large aperture array.

I. INTRODUCTION

Localization is expected to be integrated into the communication systems due to the increased bandwidth and array size with mmWave/THz band signals [1]. A by-product of localization is the estimated position of surrounding objects or scattering points (SPs) from non-line-of-sight (NLOS) paths, which is usually called (bi-/multi-static) sensing. In the 3rd Generation Partnership Project (3GPP) project, positioning in the 5G new radio (NR) has been studied in TR38.855 [2], followed by an expanded study in TR38.895 [3]. In the meantime, many theoretical analysis and experimental studies have also been carried out, both showing huge potentials of localization and sensing (L&S) in communication systems [4]–[6]. Consequently, such integration can provide vast opportunities for Internet-of-Things applications, augmented reality, smart cities, and other new use cases [7].

Due to the preferable simplicity, the mmWave channels are usually modeled with the far field (FF) assumption, based on which multi-dimensional signal processing algorithms such as ESPRIT can be adopted to extract the channel parameters of interest [8], [9]. The angle/delay information (from phase changes across antennas/subcarriers) of the line-of-sight (LOS) path and NLOS paths provide the position information of the target and the incident points (e.g., scatter points or objects), respectively [8]. However, the FF assumption is no longer valid for extremely-large antenna array (ELAA) and wideband systems [10], [11]. Communications, as well as L&S tasks

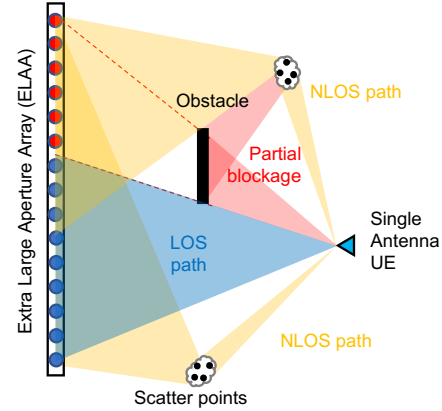


Fig. 1. Illustration of localization and sensing under partial blockage.

that are performed in the near field (NF) experience channel features such as spatial non-stationarity (SNS), beam squint effect (BSE), and spherical wave model (SWM) [10].

When adopting a FF model that ignores these features, model mismatch happens, and L&S performance will be affected [12]. However, when considering these features, extra geometrical information can be obtained, although at the cost of increased channel model complexity. For example, localization in the NF can be performed with narrowband signals by exploiting the curvature of arrival (COA) [13], even under LOS blockage [14], [15]. When considering wideband signals, joint localization and synchronization can be performed [16]. The BSE can also be utilized for coverage enhancement thanks to the spatial diversity spanned by different subcarriers (i.e., squinted beams) [17]. Hence, involving more accurate NF channel models and developing corresponding signal processing algorithms are needed.

In addition to the NF model, another issue accompanying the large array is the partial blockage of the antennas. Unlike the FF model where the antenna array is treated as a point target, and the whole antenna's blockage is considered if an object exists between the transmitter and the receiver, partial blockage indicates that a portion of antennas is affected. Similar research works have studied antenna diagnosis [18] and RIS pixel failures [14], where only few antennas are impaired. However, a larger portion of antennas might be affected by blockage, depending on the position and shape of the obstacles between the transmitter and receivers, making the detection problem challenging for analog arrays.

In this work, we study the L&S in the NF and consider partial blockage of the ELAA. The contributions of this work can be summarized as follows: (i) a NF joint synchronization, localization, and sensing problem under a stationary scenario is formulated in an uplink single-input-multiple-output (SIMO) system with a single base station (BS), which was previously not possible using a FF model; (ii) the effect of partial blockage on localization is evaluated based on the Kullback–Leibler divergence (KLD) metric; (iii) a partial blockage detection (PBD) algorithm is developed to detect blocked antennas in an analog or hybrid array with a limited number of transmissions.

II. SYSTEM MODEL

This section describes the signal and channel models of the localization system. We consider a 2D uplink SIMO system with L SPs. An N -antenna BS is located along the y -axis with its center denoted by \mathbf{p}_B , and each antenna is located at \mathbf{b}_n ($n = 1, \dots, N$). The user equipment (UE) and the ℓ -th SP are located at \mathbf{p}_0 and \mathbf{p}_ℓ , respectively. The obstacle may appear between the transmitter and the receiver and block part of the array in the LOS and NLOS paths, as seen in Fig. 1. For the convenience of performance analysis, we start with a simple scenario by adopting a point-target model of the SP. More realistic and complicated models, such as circular targets or extended targets [19] can be considered in future works.

A. Signal Model

An orthogonal frequency division multiplexing (OFDM)-based transmission is adopted in this system with K subcarriers and G transmissions. Given the transmitted signal symbol for the k -th subcarrier and g -th transmission $x_{g,k}$ ($|x_{g,k}| = \sqrt{P}$ with P as the average transmit power), the received signals can be expressed as

$$\mathbf{y}_{g,k} = \mathbf{W}_g \mathbf{h}_k x_{g,k} + \mathbf{W}_g \mathbf{n}_{g,k}. \quad (1)$$

Here, $\mathbf{y}_{g,k} \in \mathbb{C}^M$ with M as the number of radio frequency chains (RFCs), $\mathbf{h}_k \in \mathbb{C}^N$ is the channel vector of the k -th subcarrier that is assumed to be coherent during the G transmissions, $\mathbf{n}_{g,k} \in \mathcal{CN}(\mathbf{0}_N, N_0 W \mathbf{I}_N)$ is the noise vector with N_0 as the noise power spectral density (PSD) and W as the bandwidth, $\mathbf{W}_g \in \mathbb{C}^{M \times N}$ is the combining matrix that differs depending on array architectures.¹ For array-of-subarray (AOSA) structures and assume N_S is the number of antennas for all the S sub-arrays (SAs) ($N = SN_S$), the combiner can be expressed as $\mathbf{W}_g = \text{blkdiag}(\mathbf{w}_{g,1}^\top, \dots, \mathbf{w}_{g,S}^\top) \in \mathbb{C}^{S \times N}$ with $\mathbf{w}_{g,s} \in \mathbb{C}^S$ ($s = 1, \dots, S$) as the combiner vector of each SA, $(\cdot)^\top$ as the transpose operation, and $\text{blkdiag}(\cdot)$ indicating the block diagonal operation. In this work, we adopt the AOSA structure with S SAs with each of them connected to a specific RFC (the number of RFCs M equals to S).

¹For digital arrays, $\mathbf{W}_g = \mathbf{I}_N$ ($M = N$) and can thus be removed. For fully connected hybrid arrays consisting M_R RFCs, $\mathbf{W}_g \in \mathbb{C}^{S \times N}$ with each element $|w_{i,j}| = \frac{1}{\sqrt{N}}$.

B. Far Field Channel Model

When considering the FF scenario, the channel vector for the k -th subcarrier $\mathbf{h}_k^{\text{FF}} \in \mathbb{C}^N$ can be formulated as

$$\mathbf{h}_k^{\text{FF}} = \sum_{\ell=0}^L \mathbf{h}_{\ell,k}^{\text{FF}} = \sum_{\ell=0}^L \alpha_\ell \mathbf{a}_\ell(\vartheta_\ell) D_k(\tau_\ell), \quad (2)$$

where L is the number of paths, $\ell = 0$ indicates the LOS path and $\ell > 0$ corresponds to the ℓ -th NLOS path. For the ℓ -th path ($\ell = 0, \dots, L$), α_ℓ , $\mathbf{a}_\ell(\vartheta_\ell)$, $D_k(\tau_\ell)$ are the complex channel gain, FF steering vector, and delay component at the k -th subcarrier, respectively, with ϑ_ℓ and τ_ℓ as the angles-of-arrival (AOA) and delay of the ℓ -th path. More specifically,

$$\alpha_\ell = \rho_\ell e^{-j\xi_\ell} = \begin{cases} \frac{\lambda_c e^{-j\xi_\ell}}{4\pi \|\mathbf{p}_0 - \mathbf{p}_B\|} & \ell = 0, \\ \sqrt{\frac{c_\ell}{4\pi}} \frac{\lambda_c e^{-j\xi_\ell}}{4\pi \|\mathbf{p}_0 - \mathbf{p}_\ell\| \|\mathbf{p}_\ell - \mathbf{p}_B\|} & \ell > 0, \end{cases} \quad (3)$$

$$\mathbf{a}_\ell(\vartheta_\ell) = [e^{-j\pi \frac{N-1}{2} \sin(\vartheta_\ell)}, \dots, 1, \dots, e^{-j\pi \frac{1-N}{2} \sin(\vartheta_\ell)}]^\top, \quad (4)$$

$$D_k(\tau_\ell) = e^{-j\frac{2\pi}{\lambda_k} \tau_\ell} = \begin{cases} e^{-j\frac{2\pi}{\lambda_k} (\|\mathbf{p}_0 - \mathbf{p}_B\| + \beta)} & \ell = 0, \\ e^{-j\frac{2\pi}{\lambda_k} (\|\mathbf{p}_0 - \mathbf{p}_\ell\| + \|\mathbf{p}_\ell - \mathbf{p}_B\| + \beta)} & \ell > 1, \end{cases} \quad (5)$$

where λ_c and λ_k are the wavelengths corresponding to the central frequency and the k -th subcarrier, and c_ℓ is the Radar cross section of the ℓ -th path. Due to the unknown clock offset β in τ_ℓ , localization cannot be performed in a SIMO system with a single BS under FF scenarios, even with wideband signals.

C. Near-field Channel Model

By adopting a NF model, the channel vector \mathbf{h}_k^{NF} can then be formulated as

$$\mathbf{h}_k^{\text{NF}} = \sum_{\ell=0}^L \alpha_{\ell,k}(\mathbf{p}_\ell) \odot \mathbf{m}_\ell \odot \mathbf{d}_{\ell,k}(\mathbf{p}_\ell) D_{\ell,k}(\mathbf{p}_0, \mathbf{p}_\ell, \beta), \quad (6)$$

where $\mathbf{m}_\ell \in \mathbb{R}^N$ is the masking vector with each element as either 1 (unblocked) or 0 (blocked). Diffraction may happen depending on the shape and materials of the object and cause non-zero coefficients for the blocked antennas [20], which will be evaluated in the simulation. The frequency-dependent NF channel gain, steering vector, and delay component $\alpha_{\ell,k}$, $\mathbf{d}_{\ell,k}$, and $D_{\ell,k}$ can be expressed as

$$\alpha_{\ell,k,n}(\mathbf{p}_\ell) = \alpha_\ell c_{\ell,k,n}(\mathbf{p}_\ell), \quad c_{\ell,k,n}(\mathbf{p}_\ell) = \frac{\lambda_k \|\mathbf{p}_\ell - \mathbf{p}_B\|}{\lambda_c \|\mathbf{p}_\ell - \mathbf{b}_n\|}, \quad (7)$$

$$\mathbf{d}_{\ell,k,n}(\mathbf{p}_\ell) = e^{-j\frac{2\pi}{\lambda_k} (\|\mathbf{p}_\ell - \mathbf{b}_n\| - \|\mathbf{p}_\ell - \mathbf{p}_B\|)}, \quad (8)$$

$$D_{\ell,k}(\mathbf{p}_0, \mathbf{p}_\ell, \beta) = \begin{cases} e^{-j\frac{2\pi}{\lambda_k} (\|\mathbf{p}_0 - \mathbf{p}_B\| + \beta)} & \ell = 0, \\ e^{-j\frac{2\pi}{\lambda_k} (\|\mathbf{p}_0 - \mathbf{p}_\ell\| + \|\mathbf{p}_\ell - \mathbf{p}_B\| + \beta)} & \ell > 1. \end{cases} \quad (9)$$

Note that equations (9) and (5) are identical, and the near-field features are reflected on (7) and (8).

III. LOCALIZATION AND SENSING

In this section, we describe the L&S algorithms that ignore the blockage of the antennas (i.e., assuming no blockage with $\mathbf{m}_\ell = \mathbf{1}_N$), and the PBD is detailed in Sec. IV. The L&S problem can be formulated as estimating the state vector $\mathbf{s}_N = [\alpha_0, \mathbf{p}_0^\top, \dots, \alpha_L, \mathbf{p}_L^\top, \beta]^\top$ from the observed signal vector $\mathbf{y} = [\mathbf{y}_1^\top, \dots, \mathbf{y}_S^\top]^\top \in \mathbb{C}^{SGK}$ of an AOSA system with $\mathbf{y}_s = [y_{1,1,s}, \dots, y_{1,K,s}, y_{2,1,s}, \dots, y_{G,K,s}]^\top \in \mathbb{C}^{GK}$. Usually, the complex channel gains α_ℓ ($\ell = 0, \dots, L$) are treated as nuisance parameters, and the nuisance-free state vector can be expressed as $\mathbf{s} = [\mathbf{p}_0^\top, \dots, \mathbf{p}_L^\top, \beta]^\top$. Next, we propose a multi-stage L&S algorithm to provide coarse positions of the UE and SPs, and then perform position refinement using maximum likelihood estimator (MLE).

A. Coarse Localization Algorithm

1) *Localization with only LOS Path:* By segmenting the whole large array into S SAs, we can adopt available FF algorithms to estimate the AOA θ_s and delay τ_s of the s -th SA separately [21]. For the s -th SA, the estimation problem can be formulated as [22]

$$[\hat{\theta}_s, \hat{\tau}_s] = \arg \min_{\theta, \tau} \left\| \mathbf{y}_s - \frac{\mathbf{u}_s^H(\theta, \tau) \mathbf{y}_s}{\|\mathbf{u}_s(\theta, \tau)\|^2} \mathbf{u}_s(\theta, \tau) \right\|, \quad (10)$$

where $\mathbf{u}_s(\theta, \tau) = \text{vec}(\mathbf{U}_s(\theta, \tau)) \in \mathbb{R}^{GK}$ with each entry of $\mathbf{U}_s(\theta, \tau)$ as $U_{s,g,k} = \mathbf{w}_g^\top \mathbf{a}(\theta) D_k(\tau) x_{g,k}$ defined in (4) and (5), and $(\cdot)^H$ is the Hermitian operation. Note that the AOA θ and delay τ are calculated based on the center of each SA denoted as $\mathbf{p}_{SA,s}$.

Once the channel parameters for each path are estimated, we can then obtain a coarse location estimate by minimizing the distances between the UE position and all the AOA direction vectors, as

$$\hat{\mathbf{p}}_0 = \arg \min_{\mathbf{p}} \sum_{s=1}^S \|\mathbf{p}_{SA,s} + \mathbf{t}(\hat{\theta}_s)^\top (\mathbf{p} - \mathbf{p}_{SA,s}) \mathbf{t}(\hat{\theta}_s) - \mathbf{p}\|. \quad (11)$$

Here, $\mathbf{t}(\theta) = [\cos(\theta), \sin(\theta)]^\top$. A coarse clock offset $\hat{\beta}$ can also be obtained as

$$\hat{\beta} = \frac{1}{S} \sum_{s=1}^S (\hat{\tau}_s - \|\mathbf{p}_{SA,s} - \hat{\mathbf{p}}_0\|). \quad (12)$$

Finally, based on the coarse estimation from (10) and (11), an MLE problem for LOS-only NF localization can be formulated as

$$[\hat{\mathbf{p}}_0, \hat{\beta}] = \arg \min_{\mathbf{p}, \beta} \left\| \mathbf{y} - \frac{\mathbf{v}_0^H(\mathbf{p}, \beta) \mathbf{y}}{\|\mathbf{v}_0(\mathbf{p}, \beta)\|^2} \mathbf{v}_0(\mathbf{p}, \beta) \right\|, \quad (13)$$

with $\mathbf{v}_0(\mathbf{p}, \beta) = [\text{vec}(\mathbf{V}_{0,1}(\mathbf{p}, \beta))^\top, \dots, \text{vec}(\mathbf{V}_{0,S}(\mathbf{p}, \beta))^\top]^\top$ as the normalized noise-free received signal in a similar structure as \mathbf{y} , where each entry of $\mathbf{V}_{0,s}(\mathbf{p}, \beta)$ is $V_{0,s,g,k} = \mathbf{w}_g^\top (\mathbf{c}_k(\mathbf{p}) \odot \mathbf{d}_k(\mathbf{p})) D_k(\beta) x_{g,k}$.

2) Localization and Sensing with Strong NLOS Paths:

When signals from different paths are resolvable, multi-dimensional algorithms such as ESPRIT can be applied to estimate the channel parameters of each path directly [23]. By picking up the shortest path (i.e., minimum delay) as the LOS path, an initial estimate of UE position and clock bias can be obtained based on (11) and (12). Then, the position of the SPs (assuming correct channel parameters association of each SP) can be obtained as

$$\hat{\mathbf{p}}_\ell = \arg \min_{\mathbf{p}} \left[\begin{array}{c} \hat{\theta}_\ell - \boldsymbol{\theta}_{SA}(\mathbf{p}) \\ \hat{\tau}_\ell - \boldsymbol{\tau}_{SA}(\mathbf{p}) - \hat{\beta} \end{array} \right] \mathcal{I}_{\eta_\ell} \left[\begin{array}{c} \hat{\theta}_\ell - \boldsymbol{\theta}_{SA}(\mathbf{p}) \\ \hat{\tau}_\ell - \boldsymbol{\tau}_{SA}(\mathbf{p}) - \hat{\beta} \end{array} \right]^\top, \quad (14)$$

where $\hat{\theta}_\ell = [\hat{\theta}_{\ell,1}, \dots, \hat{\theta}_{\ell,S}]^\top$ and $\hat{\tau}_\ell = [\hat{\tau}_{\ell,1}, \dots, \hat{\tau}_{\ell,S}]^\top$ are the estimated channel parameters of the ℓ -th path. Vectors $\boldsymbol{\theta}_{SA}(\mathbf{p}) = [\theta_{SA,1}(\mathbf{p}), \dots, \theta_{SA,S}(\mathbf{p})]$ with $\theta_{SA,s}(\mathbf{p}) = \text{atan2}(p_1 - p_{SA,s,1}, p_2 - p_{SA,s,1})$, and $\boldsymbol{\tau}_{SA}(\mathbf{p}) = [\tau_{SA,1}(\mathbf{p}), \dots, \tau_{SA,S}(\mathbf{p})]$ with $\tau_{SA,s}(\mathbf{p}) = \|\mathbf{p}_{SA,s}(\mathbf{p}) - \mathbf{p} - \hat{\beta}\|$ are the angle and delay information at SAs for a given \mathbf{p} . The weighting matrix \mathcal{I}_{η_ℓ} can be selected based on the statistical information of the channel parameters $[\hat{\theta}_\ell^\top, \hat{\tau}_\ell^\top]$. However, the NLOS paths are usually much weaker than the LOS path, and the corresponding L&S algorithm will be presented next.

3) Localization and Sensing with Weak NLOS Paths:

Considering the NLOS path is much weaker, we need to remove the LOS path from the signal and estimate SPs from the residual signals defined as

$$\tilde{\mathbf{y}} = \mathbf{y} - \frac{\mathbf{u}^H(\hat{\theta}_0, \hat{\tau}_0) \mathbf{y}_s}{\|\mathbf{u}(\hat{\theta}_0, \hat{\tau}_0)\|^2} \mathbf{u}(\hat{\theta}_0, \hat{\tau}_0), \quad (15)$$

where $\hat{\theta}_0 = [\hat{\theta}_{0,1}, \dots, \hat{\theta}_{0,S}]$ and $\hat{\tau}_0 = [\hat{\tau}_{0,1}, \dots, \hat{\tau}_{0,S}]$ contains channel parameters of the LOS path that can be obtained based on (10) to (13), $\mathbf{u} = [\mathbf{u}_1^\top, \dots, \mathbf{u}_S^\top]$ is the concatenation of the normalized noise-free received signal at each SA. The estimation of SPs can be performed based on (14) using the residual signals obtained in (15).

B. Maximum Likelihood Estimator

Once a coarse estimation of the state vectors \mathbf{s} is obtained, we can then formulate a MLE problem similarly to (13) as

$$\hat{\mathbf{s}} = \arg \min_{\mathbf{s}} \|\mathbf{y} - \boldsymbol{\Upsilon}(\mathbf{s}) \mathbf{g}(\mathbf{s})\|, \quad (16)$$

where $\mathbf{g}(\mathbf{s}) = (\boldsymbol{\Upsilon}^H(\mathbf{s}) \boldsymbol{\Upsilon}(\mathbf{s}))^{-1} \boldsymbol{\Upsilon}^H(\mathbf{s}) \mathbf{y} \in \mathbb{C}^{L+1}$ contains the gain of each identified path, $\boldsymbol{\Upsilon}(\mathbf{s}) = [\mathbf{v}_0(\mathbf{p}_0, \beta), \dots, \mathbf{v}_L(\mathbf{p}_0, \mathbf{p}_\ell, \beta)] \in \mathbb{C}^{SGK \times (L+1)}$. The ℓ -th ($\ell > 0$) vector in $\boldsymbol{\Upsilon}(\mathbf{s})$ can be expressed as $\mathbf{v}_\ell(\mathbf{p}_0, \mathbf{p}_\ell, \beta) = [\text{vec}(\mathbf{V}_{\ell,1}(\mathbf{p}_0, \mathbf{p}_\ell, \beta))^\top, \dots, \text{vec}(\mathbf{V}_{\ell,S}(\mathbf{p}_0, \mathbf{p}_\ell, \beta))^\top]^\top$, where each entry of the matrix $\mathbf{V}_{\ell,s}(\mathbf{p}_0, \mathbf{p}_\ell, \beta)$ is given by $V_{\ell,s,g,k} = \mathbf{w}_g^\top (\mathbf{c}_k(\mathbf{p}_\ell) \odot \mathbf{d}_k(\mathbf{p}_\ell)) D_k(\beta) x_{g,k}$. The Cramér-Rao bound (CRB) can be used to benchmark the algorithm performance as detailed in [24, Sec. 3.4], which will not be detailed in this work.

IV. PARTIAL BLOCKAGE DETECTION

Once the position of UE and SP are estimated, the PBD algorithm can be performed. In this section, we focus on the partial blockage of LOS path only and propose a heuristic algorithm to detect the blocked antennas.

A. The Effect of Partial Blockage

Partial blockage affects localization and sensing performance differently depending on the knowledge of the blockage. If we know the blocked antennas, the L&S performance loss is mainly due to the reduced array size (i.e., only visible antennas provide information). However, if we ignore the blockage and perform L&S tasks by assuming all the antennas are visible to the UE, model mismatches are introduced, resulting in severe performance degradation. More specifically, the estimation error can be lower bounded by [25]

$$\text{LB}(\bar{\mathbf{s}}, \mathbf{s}_0) = \text{MCRB}(\mathbf{s}_0) + (\bar{\mathbf{s}} - \mathbf{s}_0)(\bar{\mathbf{s}} - \mathbf{s}_0)^\top, \quad (17)$$

which contains an MCRB term and a biased term characterized by pseudotrue parameters \mathbf{s}_0 , with $\bar{\mathbf{s}}$ as the true state [25]. The pseudotrue parameter \mathbf{s}_0 is defined as the vector that minimizes the KLD between the probability density function of the blocked model f_B (signal model from (1) and (6)) and the assumed model f_U (i.e., by assuming no blockage with $\mathbf{m}_\ell = \mathbf{1}_N$) as

$$\mathbf{s}_0 = \arg \min_{\mathbf{s}} D_{\text{KL}}(f_B(\mathbf{y}|\bar{\mathbf{s}})||f_U(\mathbf{y}|\mathbf{s})). \quad (18)$$

At high SNR, MCRB is ignorable and the biased term dominates, which limits the fundamental mismatched error. In other words, the estimation that ignores the effect of partial blockage will introduce a biased term, resulting in a result \mathbf{s}_0 with mismatch error instead of the true state $\bar{\mathbf{s}}$.

B. Partial Blockage Problem Formulation

1) *Blockage Detection with Sufficient Observations*: It is easy to detect the partial blockage of the LOS path by simple thresholding in digital arrays. For analog and hybrid arrays, similar approaches can be applied to recover the beamspace channel to the element-space channel with sufficient observations (i.e., no less than the number of antennas in analog arrays). Take the DFT codebook in an analog array as an example; concatenating the observed signals as $\tilde{\mathbf{y}} = [\mathbf{y}_1, \dots, \mathbf{y}_G]^\top$ and multiplying by an IFFT matrix will result in an element space channel vector (with noise). When other combiner vectors are adopted (e.g., $\mathbf{W}_g \in \mathcal{R}^{M \times N}$, $M > 1$), this process can be done by multiplying a pseudoinverse matrix of $\tilde{\mathbf{W}} = [\mathbf{W}_1, \dots, \mathbf{W}_G]$ to the concatenated observations $\tilde{\mathbf{y}} = [\mathbf{y}_{1,1}, \dots, \mathbf{y}_{1,M}, \dots, \mathbf{y}_{G,M}]^\top$ to obtain an element-space channel vector, with $\mathbf{y}_{g,m}$ as the received signal of the g -th transmission at the m -th RFC.

2) *PBD with a Limited Number of Observations*: When there is only a limited number of observations (i.e., less than the number of antennas in analog arrays), the PBD task becomes challenging. If we assume the blocked antennas are adjacent to each other, the detection problem becomes feasible

by implementing a heuristic way. Specifically, we want to find the masking vector where a continuous sequence of antennas is all zeros. By considering the blockage of the LOS path (given the fact that the NLOS paths are much weaker), the problem can be formulated as finding the masking vector \mathbf{m} that minimizes the objective function $J(\hat{\mathbf{s}}, \mathbf{m})$ given by

$$\hat{\mathbf{m}} = \arg \min_{\mathbf{m}} J(\hat{\mathbf{s}}, \mathbf{m}) = \arg \min_{\mathbf{m}} \|\mathbf{y} - \tilde{\mathbf{Y}}(\hat{\mathbf{s}}, \mathbf{m})\mathbf{g}(\hat{\mathbf{s}})\|, \quad (19)$$

where $\tilde{\mathbf{Y}} = [\mathbf{u}_0(\mathbf{p}, \beta) \odot \mathbf{m}, \mathbf{u}_1, \dots, \mathbf{u}_L]$ and $\mathbf{g}(\hat{\mathbf{s}})$ is defined in (16). The detection accuracy can be defined as

$$\text{Accuracy} = 1 - \frac{\|\hat{\mathbf{m}} - \bar{\mathbf{m}}\|^2}{N}. \quad (20)$$

C. The Proposed Algorithm

The detection problem in (19) is an NP-hard integer programming. In the next, We propose a low computational complexity method for blockage detection. At the first step, we assume only one antenna is blocked, resulting in $N_S + 1$ different candidate masking vectors $\mathbf{m}_{<0>}, \dots, \mathbf{m}_{<N_S>}$ (where $\mathbf{m}_{<0>}$ has all ones except the i -th element as zero, and $\mathbf{m}_{<0>} = \mathbf{1}_N$). By calculating the cost based on (19), the masking vector with the lowest value will be considered, and the blockage index is denoted as i_C . Note that if the vector $\mathbf{m}_{<0>}$ has the lowest cost, no blockage happens. Starting from $\mathbf{m}_{<0>}$, we evaluate the masking vectors by including left elements $\mathbf{m}_{<i:i_C>}$ (where $\mathbf{m}_{<i:j>}$ has all ones except the i -th to j -th entries), until the cost function is not decreasing or reaching the first element and we denote the leftmost blocked antenna as i_L . Similar can be performed for $\mathbf{m}_{<i_L:i>}$ by incorporating the right antennas, and $\mathbf{m}_{<i_L:i_R>}$ will be taken as the masking vector. Once the masking vector has been obtained, the localization and sensing results can also be refined iteratively. The algorithm can be found in Algorithm 1.

Algorithm 1 Partial Blockage Detection

```

1: — Heuristic Detection —
2: Input:  $\tilde{\mathbf{Y}}, \hat{\mathbf{s}}$ 
3:  $i_C = \arg \min_i J(\hat{\mathbf{s}}, \mathbf{m}_{<i>})$  ( $i = 0, 1, \dots, N$ ) using (19)
4: if  $i_C \neq 0$  then
5:    $i_L \leftarrow i_C, i_R \leftarrow i_C$ 
6:   if  $i_L \neq 1$  then
7:      $i_L = \arg \min_i J(\hat{\mathbf{s}}, \mathbf{m}_{<i:i_C>})$  ( $i = 1, \dots, i_C - 1$ )
8:   if  $i_R \neq N$  then
9:      $i_R = \arg \min_i J(\hat{\mathbf{s}}, \mathbf{m}_{<i_L:i>})$  ( $i = i_C + 1, \dots, N$ )
10:  return  $\hat{\mathbf{m}} \leftarrow \mathbf{m}_{<i_L:i_R>}$ 
11: — Iterative Refinement (Optional) —
12: Estimate the state vector  $\hat{\mathbf{s}}$  by solving (16) with  $\mathbf{y}, \hat{\mathbf{m}}$  as inputs.
13: Repeat steps 1-8 for a refined  $\hat{\mathbf{m}}$ 

```

V. SIMULATION

We consider a 28 GHz system with a bandwidth $W = 200$ MHz, and $K = 10$ subcarriers for localization. A single-antenna UE located at $\mathbf{p}_0 = [2, 4]^\top \text{m}$ and one SP located at $\mathbf{p}_1 = [2, -2]^\top \text{m}$, and the array size is set as $N = 100$. For reference, the Fresnel distance and Fraunhofer distance are 2.2 m and 50 m, respectively. We assume $M = 4$ RFCs are

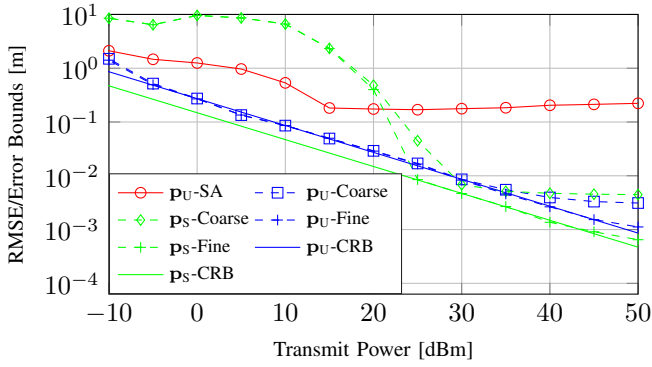


Fig. 2. RMSE of the estimated UE and SP positions.

connected to $S = 4$ SAs (e.g., the first SA contains antennas 1-25), and the number of transmissions is set as $G = 25$. The RCS coefficient for the SP is set as $c_{\text{RCS}} = 0.5 \text{ m}^2$, noise figure is set as 13 dBm, and the noise PSD is set as -173.855 dBm/Hz .

A. Evaluation of the Estimator

We evaluate the root mean squared error (RMSE) of the estimated UE and SP positions with different estimators, as shown in Fig. 2. The figure shows that the SA-based solution in (11) provides limited accuracy. With coarse estimation based on (13), \mathbf{p}_U estimation can be improved but will deviate from the bound at high SNR due to the ignorance of weak NLOS path. Similar can be found in SP position results, where the deviation happens because of the residual error of LOS removal. However, with joint optimization of both paths based on (16), the RMSEs can attain the bound. Note that we assume the number of SPs is known, and a wrong number of L will degrade localization and sensing performance. Compared with the RMSE of UE position that can provide good estimations at -10 dBm , satisfactory sensing results can only be obtained at high frequencies due to the weak signals that are easy to be interfered with by the LOS signal and background noise. Finally, the CRB of \mathbf{p}_U and \mathbf{p}_S are plotted in the black curve to benchmark the estimators.

B. Effect of Partial Blockage

To evaluate the effect of partial blockage on localization in terms of the biased term. The UE is located on a grid within a $5 \times 16 \text{ m}^2$ with an 1 m interval. The pseudotrue locations are plotted in red, with the segment representing the Biased term. In (a), where only one antenna is blocked, we find that the effect is ignorable. When more antennas are blocked, we can see that the target at a large angle of AOA will be affected more severely, and the biased term at different locations shows a different pattern. When a partial blockage happens at different locations, we can see that the blockage of middle antennas has less effect on localization, indicating less bias introduced. As a result, detecting partial blockage and identifying blocked antennas can help in localization and sensing.

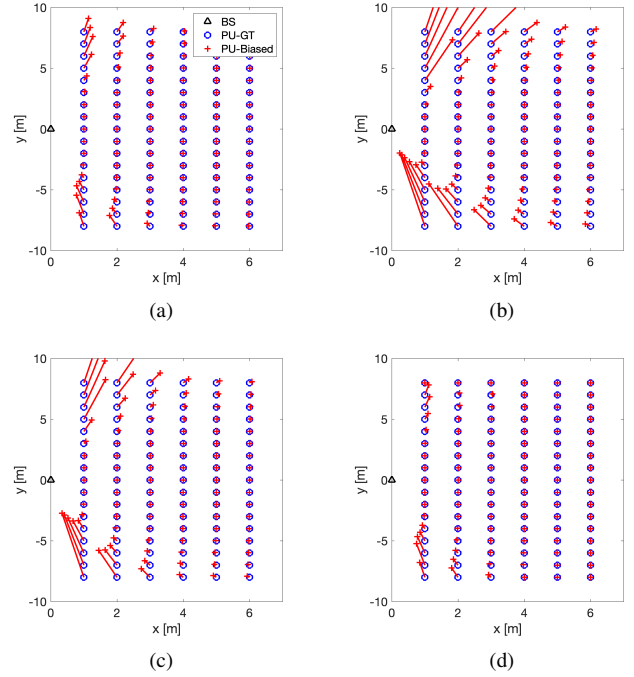


Fig. 3. The effect of partial blockage on localization under different scenarios (blue circle indicates the ground truth and the red cross indicates the biased estimation): (a) antenna 100 is blocked; (b) antennas 96-100 are blocked; (c) antennas 76-80 are blocked; (d) antennas 56-60 are blocked.

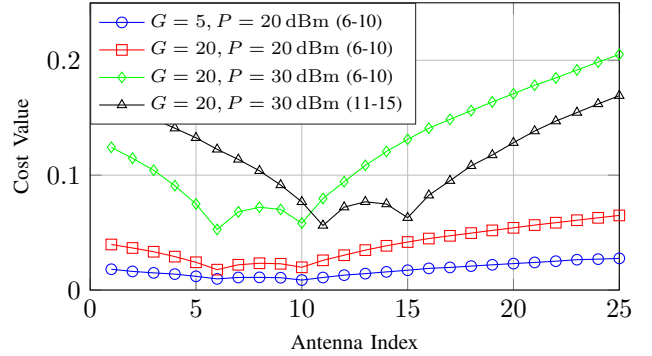


Fig. 4. Cost function of the heuristic algorithm (with partial blockage in antennas 6-10 and 11-15).

C. Evaluation of Partial Blockage Detection Algorithm

The cost function after performing steps 1-9 in Algorithm 1 is shown in Fig. 4 (averaged with 100 times Monte Carlo simulations). From the benchmark scenario with a limited number of transmission and transmit power (blue curve with circle markers), the averaged cost values are close to each other, indicating an inaccurate detection is likely to happen. With increased transmissions (red curves with square markers), two local minima (antenna index 6 and 10) are more visible, indicating the boundary of the blocked antennas. The averaged cost functions with higher transmit power for different blocked antennas (green curve with diamond markers and black curve with triangle markers) are also shown in the figure, indicating these setups are likely to be successfully detected.

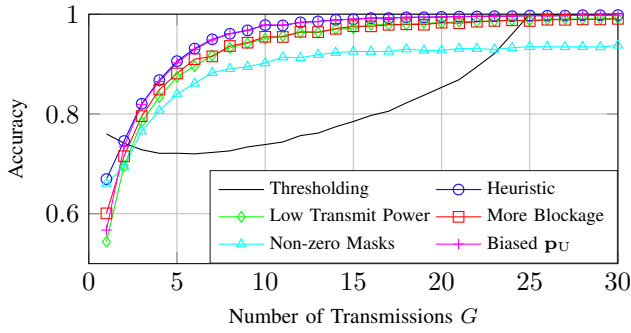


Fig. 5. The evaluation of the PBD methods under different scenarios.

We take the first SA with antenna index 1-25) to evaluate two different partial blockage methods with different known UE locations (i.e., a true location and a biased location). The default parameters are set as $P = 20$ dBm, $c = 0.5$ m², with antennas 5-10 in the SA blocked as the benchmark. Other scenarios such as lower power ($P = 0$ dBm), non-zero masks (the coefficient follows $\mathcal{CN}(0.2, 0.2)$ instead of 0) and more blockage (antennas 5-15 are blocked), biased $\mathbf{p} = [2.0691, 4.1377]^T$ m (based on (18)) are also evaluated. We can see that the thresholding method (black curve) only works for a sufficient number of transmissions ($G \geq 25$), and accuracy decreases with a reduced value of G . When $G = 1$, no blocked antennas can be detected, resulting in a constant value of $1 - 6/25 = 0.76$. However, the heuristic method (blue curve) shows a much-improved performance. The results also show that a lower transmit power, more blockages, and a wrong assumption of the masking vector decrease detection accuracy. However, a biased position estimate has a limited effect on the accuracy due to the fact that the biased position minimizes the KLD, providing similar signal observations as the ground truth positions.

VI. CONCLUSION

In this work, we studied a SIMO uplink joint synchronization, localization, and sensing problem in the NF scenario with a single BS, which was previously impossible with a far-field model. A subarray-based coarse localization and sensing algorithm is performed, followed by an MLE-based refinement. We also analyzed the impact of localization under partial blockage and proposed a heuristic blockage detection algorithm to mitigate the effect of blockage. However, the reflection and diffraction of the blockage itself are not considered, and joint localization and PBD in 3D space need to be considered in future work.

ACKNOWLEDGMENT

This work has been supported by the SNS JU project 6G-DISAC under the EU's Horizon Europe research and innovation programme under Grant Agreement No 101139130.

REFERENCES

[1] A. Behravan *et al.*, "Positioning and sensing in 6G: Gaps, challenges, and opportunities," *IEEE Veh. Technol. Mag.*, vol. 18, no. 1, pp. 40–48, Mar. 2023.

[2] "3GPP TR 38.855 V16.0.0: Study on NR positioning support (Release 16) (accessed on 28-Jan-2024)," Mar. 2019. [Online]. Available: <https://portal.3gpp.org/desktopmodules/Specifications/SpecificationDetails.aspx?specificationId=3501>

[3] "3GPP TR 38.859 V18.0.0: Study on NR positioning support (Release 18) (accessed on 28-Jan-2024)," Jan. 2023. [Online]. Available: <https://portal.3gpp.org/desktopmodules/Specifications/SpecificationDetails.aspx?specificationId=3985>

[4] K. Gao *et al.*, "Toward 5G NR high-precision indoor positioning via channel frequency response: A new paradigm and dataset generation method," *IEEE J. Sel. Areas Commun.*, vol. 40, no. 7, pp. 2233–2247, Mar. 2022.

[5] Y. Ruan *et al.*, "iPos-5G: Indoor positioning via commercial 5G NR CSI," *IEEE Internet Things J.*, vol. 10, no. 10, pp. 8718–8733, Dec. 2022.

[6] Y. Ge *et al.*, "Experimental validation of single BS 5G mmWave positioning and mapping for intelligent transport," *arXiv preprint arXiv:2303.11995*, 2023.

[7] F. Liu *et al.*, "Integrated sensing and communications: Towards dual-functional wireless networks for 6G and beyond," *IEEE J. Sel. Areas Commun.*, vol. 40, no. 6, pp. 1728–1767, Jun. 2022.

[8] F. Roemer *et al.*, "Analytical performance assessment of multi-dimensional matrix-and tensor-based ESPRIT-type algorithms," *IEEE Trans. Signal Process.*, vol. 62, no. 10, pp. 2611–2625, Mar. 2014.

[9] P. Zheng *et al.*, "JrCUP: Joint RIS calibration and user positioning for 6G wireless systems," *IEEE Trans. Wireless Commun.*, Dec. 2023.

[10] H. Chen *et al.*, "6G localization and sensing in the near field: Features, opportunities, and challenges," *IEEE Wireless Commun.*, 2024.

[11] A. Elzanaty *et al.*, "Towards 6G holographic localization: Enabling technologies and perspectives," *IEEE Internet of Things Magazine*, vol. 6, no. 3, pp. 138–143, Sep. 2023.

[12] H. Chen *et al.*, "Channel model mismatch analysis for XL-MIMO systems from a localization perspective," in *Proc. IEEE Global Commun. Conf. (GLOBECOM)*, Dec. 2022, pp. 1588–1593.

[13] A. Guerra *et al.*, "Near-field tracking with large antenna arrays: Fundamental limits and practical algorithms," *IEEE Trans. Signal Process.*, vol. 69, pp. 5723–5738, Aug. 2021.

[14] C. Ozturk *et al.*, "RIS-aided near-field localization under phase-dependent amplitude variations," *IEEE Trans. Wireless Commun.*, vol. 22, no. 8, pp. 5550–5566, Aug. 2023.

[15] O. Rinchi *et al.*, "Single-snapshot localization for near-field RIS model using atomic norm minimization," in *Proc. IEEE Global Commun. Conf. (GLOBECOM)*, Dec. 2022, pp. 2432–2437.

[16] D. Dardari *et al.*, "LOS/NLOS near-field localization with a large reconfigurable intelligent surface," *IEEE Trans. Wireless Commun.*, vol. 21, no. 6, pp. 4282–4294, Nov. 2021.

[17] M. Cui *et al.*, "Near-field rainbow: Wideband beam training for XL-MIMO," *IEEE Trans. Wireless Commun.*, vol. 22, no. 6, pp. 3899–3912, Jun. 2023.

[18] R. Sun *et al.*, "Blind diagnosis for millimeter-wave large-scale antenna systems," *IEEE Commun. Lett.*, vol. 25, no. 7, pp. 2390–2394, Apr. 2021.

[19] N. Garcia *et al.*, "Cramér-Rao bound analysis of radars for extended vehicular targets with known and unknown shape," *IEEE Trans. Signal Process.*, vol. 70, pp. 3280–3295, Jun. 2022.

[20] C. Han *et al.*, "Multi-ray channel modeling and wideband characterization for wireless communications in the terahertz band," *IEEE Trans. Wireless Commun.*, vol. 14, no. 5, pp. 2402–2412, May. 2015.

[21] H. Wymeersch, "A Fisher information analysis of joint localization and synchronization in near field," in *Proc. IEEE Int. Conf. Commun. (ICC Workshops)*. IEEE, Jun. 2020.

[22] H. Chen *et al.*, "Modeling and analysis of OFDM-based 5G/6G localization under hardware impairments," *IEEE Trans. Wireless Commun. (Early Access)*, Dec. 2023.

[23] F. Wen *et al.*, "5G positioning and mapping with diffuse multipath," *IEEE Trans. Wireless Commun.*, vol. 20, no. 2, pp. 1164–1174, Oct. 2020.

[24] S. M. Kay, *Fundamentals of statistical signal processing: estimation theory*. Prentice-Hall, Inc., 1993.

[25] S. Fortunati *et al.*, "Performance bounds for parameter estimation under misspecified models: Fundamental findings and applications," *IEEE Signal Process. Mag.*, vol. 34, no. 6, pp. 142–157, Nov. 2017.